Ringwoodite lamellae in olivine: Clues to olivine–ringwoodite phase transition mechanisms in shocked meteorites and subducting slabs

Ming Chen*†, Ahmed El Goresy‡, and Philippe Gillet§

*Guangzhou Institute of Geochemistry, Chinese Academy of Sciences, Guangzhou 510640, China; ‡Max-Planck-Institut für Chemie, 55128 Mainz, Germany; and §Laboratoire des Sciences de la Terre, Centre National de la Recherche Scientifique, Unité Mixte de Recherche 5570, Ecole Normale Supérieure de Lyon, 46 Allée d'Italie, 69364 Lyon Cedex 7, France

Edited by Ho-kwang Mao, Carnegie Institution of Washington, Washington, DC, and approved September 15, 2004 (received for review July 12, 2004)

The first natural occurrence of ringwoodite lamellae was found in the olivine grains inside and in areas adjacent to the shock veins of a chondritic meteorite, and these lamellae show distinct growth mechanism. Inside the veins where pressure and temperature were higher than elsewhere, ringwoodite lamellae formed parallel to the {101} planes of olivine, whereas outside they lie parallel to the (100) plane of olivine. The lamellae replaced the host olivine from a few percent to complete. Formation of these lamellae relates to a diffusion-controlled growth of ringwoodite along shear-induced planar defects in olivine. The planar defects and ringwoodite lamellae parallel to the {101} planes of olivine should have been produced in higher shear stress and temperature region than that parallel to the (100) plane of olivine. This study suggests that the time duration of high pressure and temperature for the growth of ringwoodite lamellae might have lasted at least for several seconds, and that an intracrystalline transformation mechanism of ringwoodite in olivine could favorably operate in the subducting lithospheric slabs in the deep Earth.

Natural ringwoodite had been found in many shocked chondritic meteorites, in which the ringwoodite occurs as fine-grained polycrystalline aggregates formed through a phase transition of olivine during exogenous dynamic events on the parent asteroids (1–4). It was also suggested that the olivine–ringwoodite transformation could take place in cold subducting slabs at the deep transition zone, where pressure oversteps the ringwoodite stability field (5–9). An experiment-produced texture characteristic of this phase transition in the slabs is the formation of ringwoodite lamellae within individual olivine crystals (6, 7, 10–12). A number of laboratory experiments on compositions like Mg_2GeO_4, Fe_2SiO_4, and $(Mg,Fe)_2SiO_4$ showed that the spinel-structured lamellae lie parallel to the (100) planes of olivine (6, 10–18). These ringwoodite lamellae form platelets from several unit cells to 100 nm in thickness (6, 10–12, 14–18). The formation of ringwoodite lamellae in olivine was attributed either to a martensitic transformation mechanism (6, 13, 15–19) or an intracrystalline nucleation and growth mechanism by which coherent nucleation of ringwoodite occurs on the stacking faults of olivine (10–12). However, no natural occurrence of ringwoodite lamellae had been found so far either in the shocked meteorites or exhumed subducted slabs.

Sixiangkou meteorite is a heavily shock-metamorphosed L6-chondrite with a number of shock-produced veins up to 10 mm in thickness. The shock veins contain abundant high-pressure minerals including ringwoodite, majorite, garnet, and magnesiowüstite, for which the shock-produced pressure and temperature of ≈20 GPa and 2,000°C were inferred (4). Polycrystalline aggregates of ringwoodite and majorite up to 100 μm in size and porphyroclastic grains of olivine and pyroxene up to 1.5 mm in size distribute throughout the shock veins and are enclosed in the fine-grained matrix consisting of magnesiowüstite, majorite garnet, metal, and troilite solidified from a shock-induced chondritic melt at high pressures (Fig. 1*a*). Outside the shock veins, the chondritic portions consist of olivine, pyroxene, plagioclase glass, troilite, kamacite, taenite, and accessory minerals chromite, apatite, and whitlockite. In this article, we report the discovery of natural occurrence of ringwoodite lamellae in olivine in this meteorite.

Methods

Polished thin sections (35 μm in thickness) of Sixiangkou meteorite samples with shock-melt veins were prepared. The mineral assemblages and textures were characterized with an optical microscope and a Hitachi (Tokyo) S-3500N scanning electron microscope in back-scattered electron (BSE) mode. Compositions of minerals were quantitatively determined by a JXA-8900RL electron microprobe (JEOL) at 15-kV accelerating voltage and 10-nA sample current at Mainz University. Raman spectra were recorded with a Renishaw (Gloucestershire, U.K.) RM-2000 instrument at the Guangzhou Institute of Geochemistry. A microscope was used to focus the excitation beam (Ar^+ laser, 514-nm line) to a 2-μm spot and to collect the Raman signal. Accumulations of Raman spectra lasted from 120 to 150 s.

Results

We observed that some individual olivine crystals inside and outside the shock veins contain lamellar texture. These lamellae were studied by using an optical microscope in reflected light and by scanning electron microscopy in BSE mode, in which the lamellae display brighter than the surrounding olivine matrix. However, the textures of lamellae in olivine inside and within a region <50 μm bordering the shock veins are distinct from those in the chondritic portion but beyond the 50-μm region and at several hundred μm distance from the veins. The former usually contains two sets of lamellae, whereas the latter contains only one set. Fig. 1 depicts a porphyroclastic grain of olivine (0.6 × 0.9 mm in dimension) inside the shock vein, in which two sets of lamellae can be recognized. Individual olivine grains were replaced by lamellae from a few percent to complete. The rim of the porphyroclastic olivine ≈200 μm in width contains higher density of optically visible lamellae than the interior (Fig. 1 *c* and *d*). Widths of lamellae at the rim are also thicker (0.3–2 μm, 1.5 μm average) than that in the interior (0.05–0.5 μm, 0.2 μm average). Fig. 2 shows a single crystal of olivine in the chondritic portion at a distance ≈150 μm away from the shock vein, in which only one set of lamellae can be observed. Olivine grains with one set of lamellae usually distribute in the chondritic area close to the shock veins in a zone with a width <300 μm. Complete replacement of lamellae in the host olivine was not

This paper was submitted directly (Track II) to the PNAS office.

Abbreviation: BSE, back-scattered electron.

†To whom correspondence should be addressed. E-mail: mchen@gig.ac.cn.

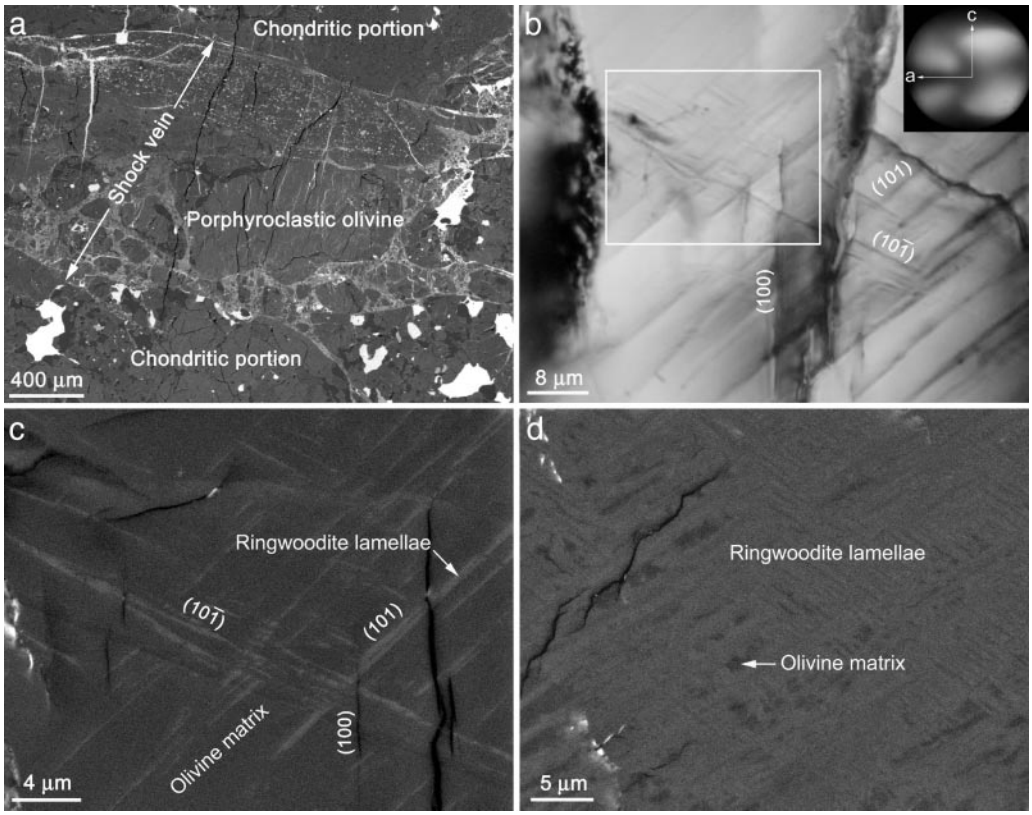

Fig. 1. The porphyroclastic grains of olivine inside the shock vein showing two sets of ringwoodite lamellae. (*a*) The BSE image shows that a shock vein intersecting the chondritic portions of meteorite contains porphyroclastic grains of silicates (olivine, pyroxene, ringwoodite, and majorite) and the fine-grained matrix consisting mainly of magnesiowüstite, garnet, metal, and troilite. (*b*) Under plane polarized light, the optical picture taken at the central part of a porphyroclastic grain of olivine in the shock vein from *a* displays three sets of planar textures parallel to the (100), (101), and (10$\bar{1}$) planes. (*Inset*) The optical biaxial interference of a negative crystal shows that the crystal lies on a position of oblique-crossing optical axes; from it the crystallographic orientation of a and c axes can be indexed. (*c*) BSE image from the frame area of *b* shows that the planar textures parallel to (101) and (10$\bar{1}$) consist of ringwoodite lamellae, whereas those parallel to (100) are open fractures. Note that the interfaces of ringwoodite lamellae are distinct but locally become broader, and that the lamellae are cut off by the (100) fractures. (*d*) The BES image shows two sets of high-density ringwoodite lamellae at the rim of a porphyroclastic olivine from *a* and >95% by volume of olivine being transformed into ringwoodite lamellae. The light gray slices represent ringwoodite lamellae, and the dark areas between the lamellae are olivine. Note that these lamellae are relatively thicker than those in the interior of porphyroclastic olivine shown in *c* and locally become broad.

observed in this type of olivine grain, and these grains contain <10% by volume of lamellae. The widths of lamellae are up to 2 μm, mostly 0.5 μm. Both kinds of lamellae occur as straight thin platelets from a few to several hundred μm in length. The interfaces of lamellae with the host olivine are distinct and become locally broaden.

The chemical compositions of the lamellae lie within the compositional range of the bulk olivine in the chondritic portion. However, the FeO content of lamellae in an individual lamellae-bearing olivine crystal is slightly but systematically higher (22.51 wt %) than that of olivine grain matrix (21.86 wt %) (Table 1). We identified the nature of the phase in the lamellae by Raman spectroscopy. Fig. 3 displays the Raman spectra obtained from a lamella in porphyroclastic grain of lamellae-bearing olivine inside the shock veins. Raman spectrum of the lamella contains two strong bands at 798 and 844 cm^{-1} and a weak band at 298 cm^{-1}, and all three bands unambiguously can be assigned to ringwoodite (20, 21), whereas the spectrum of olivine matrix of this grain displays two characteristic strong bands at 822 and 852 cm^{-1}. The weak bands at 714 and 918 cm^{-1} in the spectrum of lamella indicate the existence of traces of wadsleyite (21). Fig. 4 shows the Raman spectra of a lamellae-bearing olivine grain in the chondritic portion outside the shock vein. We note that these lamellae are too thin to obtain a pure spectrum from the lamella itself and that the spectrum taken from lamella usually depicts bands of several phases including those of the lamellae and the surrounding olivine host. We identify the spectrum of lamella as consisting mainly of ringwoodite with traces of wadsleyite, in which the strong bands at 798 and 844 cm^{-1} correspond to ringwoodite and the bands at 712 and 918 cm^{-1} correspond to wadsleyite. The other bands at 600, 822, 852, and 955 cm^{-1} appearing in the spectrum of lamella emerge from olivine (20, 21). The spectrum of olivine neighboring the

Table 1. Chemical compositions of olivine and ringwoodite lamellae (in wt %)

Oxides	Bulk olivine	Lamellae	Olivine matrix
SiO_2	38.04	38.08	38.11
MgO	38.52	37.86	38.53
CaO	0.05	0.06	0.04
Na_2O	n.d.	n.d.	n.d.
MnO	0.51	0.45	0.52
FeO	22.24	22.51	21.86
TiO_2	0.02	0.02	0.02
Al_2O_3	n.d.	n.d.	n.d.
Cr_2O_3	0.05	0.04	0.04
V_2O_3	n.d.	n.d.	n.d.
Totals	99.44	99.02	99.12

n.d., Not detected.

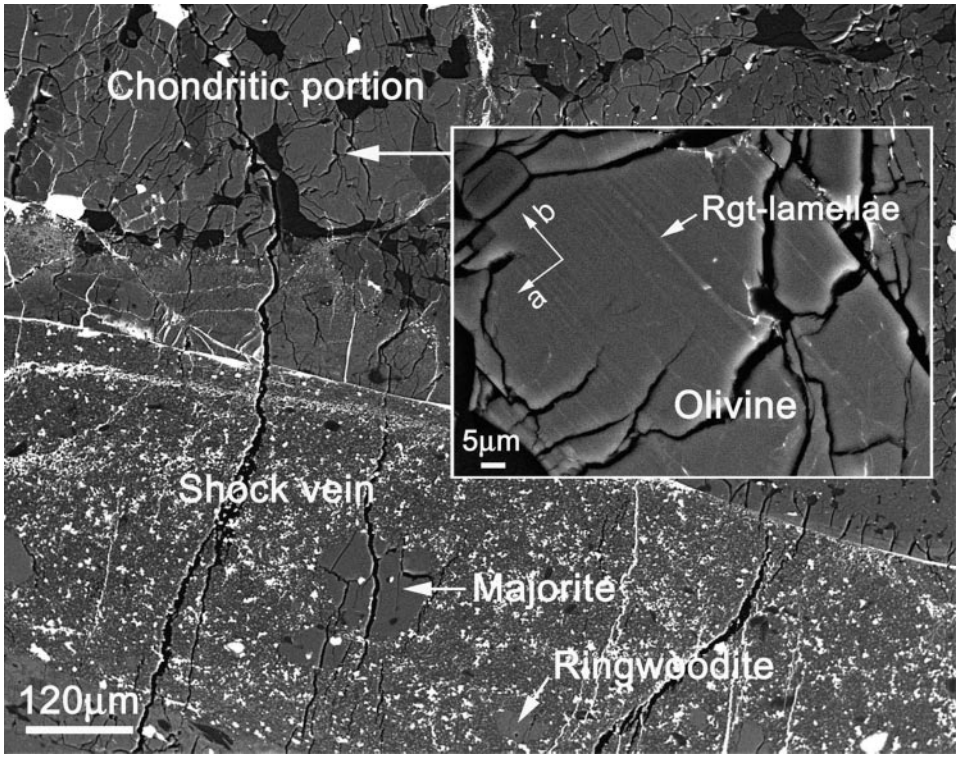

Fig. 2. A BSE image shows that a single crystal of olivine outside the shock vein contains one set of ringwoodite (Rgt) lamellae parallel to the (100) plane of olivine. Within the shock vein, there are some polycrystalline aggregates of ringwoodite and majorite.

lamellae in the same olivine grain consists of the bands at 420, 600, 822, 852, 916, and 956 cm^{-1}. These analyses demonstrate unambiguously that both lamellae occurring in olivine inside and outside the shock veins are composed mainly of ringwoodite with traces of wadsleyite. The amount of wadsleyite in lamellae is similar inside and outside the shock veins.

We were able to determine the optical orientation of the olivine slices in thin sections of sample and the orientation of ringwoodite lamellae in the host olivine crystals through study of the optical biaxial interference figures under convergent polarized light. The two sets of ringwoodite lamellae in olivine grains inside the shock veins are parallel to the {101} crystallographic planes of olivine, i.e., (101) and (10$\bar{1}$), respectively (Fig. 1 *b* and *c*). The planar fractures parallel to the (100) plane of olivine are both optically and electronically visible, but are barren of any ringwoodite lamellae along this orientation at the resolution of SEM (0.05 μm). Some {101} lamellae are cut off by the (100) fractures. In the chondritic portion, one set of ringwoodite lamellae in olivine grains lies parallel to the (100) crystallographic planes of olivine (Fig. 2). It is worth a further investigation to scrutinize whether there are nanometer-scaled lamellae parallel to both {101} and (100) planes of olivine in both grains inside and outside the shock veins.

Discussion

Mechanically deformed olivine grains usually exhibit planar defects (stacking faults and fractures) in the slip systems {110}[001], {0*kl*}[100], and (100). The slip system on {110}[001] in olivine was reported in naturally shocked meteorites that experienced low-moderate temperatures (500–800°C) and high strain rates (22). The slip system on {0*kl*}[100] identified in the terrestrial mantle rocks experienced high temperatures (1,000°C) and low strain rates (23, 24). Abundant stacking faults parallel to the (100) plane of olivine were produced in laboratory experiments by using a multianvil device at pressures between 18 and 20 GPa and temperatures 900–1,400°C (10, 12). However, the planar defects parallel to {101}[010] of olivine were not reported previously from either naturally or experimentally deformed olivine.

The transformation of olivine to ringwoodite is reconstructive and could not proceed completely by a martensitic mechanism because the cations in olivine cannot be moved to the positions in ringwoodite (25). It is possible that a number of deformation features, presumably the {101} and (100) planar defects, should have been developed in some deformed olivine of the Sixiangkou meteorite during the impact event. The planar defects developed in olivine provide nucleation sites for ringwoodite (11, 12). The straight lamellae of ringwoodite support a shear-promoted coherent nucleation and growth of the lamellae along planar defects in olivine. The relatively higher FeO content in the ringwoodite lamellae in comparison with a lower FeO content in the host olivine matrix supports compositional diffusion of Fe during nucleation and growth of ringwoodite lamellae.

During a shock, shear stresses may be created everywhere in the meteorite, but they should be much higher and concentrated in zones where the shock melt veins formed in response to reverberation effects or difference in elastic impedance between minerals. Formation of shock veins in meteorites is thus currently attributed to shear faulting and frictional melting under differential stress (26). Lenses of wadsleyite/ringwoodite lying parallel to (101) of olivine were experimentally produced by Kerschhofer *et al.* (11, 12), but no lamellae of wadsleyite/ringwoodite parallel to this crystallographic orientation of olivine were found in their experiments. The formation of the {101} defects in olivine could represent an alternative nucleation mechanism, which is active only at higher temperatures (1,500–2,000°C). A two-stage process can be proposed. First, the {101} defects are produced in the high-stress region where the shock veins will be formed, whereas the (100) defects are produced in olivine grains far from the forming shock veins in zones where the stress is lower. Then, the olivine grains containing the {101} defects that act as nucleation sites are entrained in the vein where

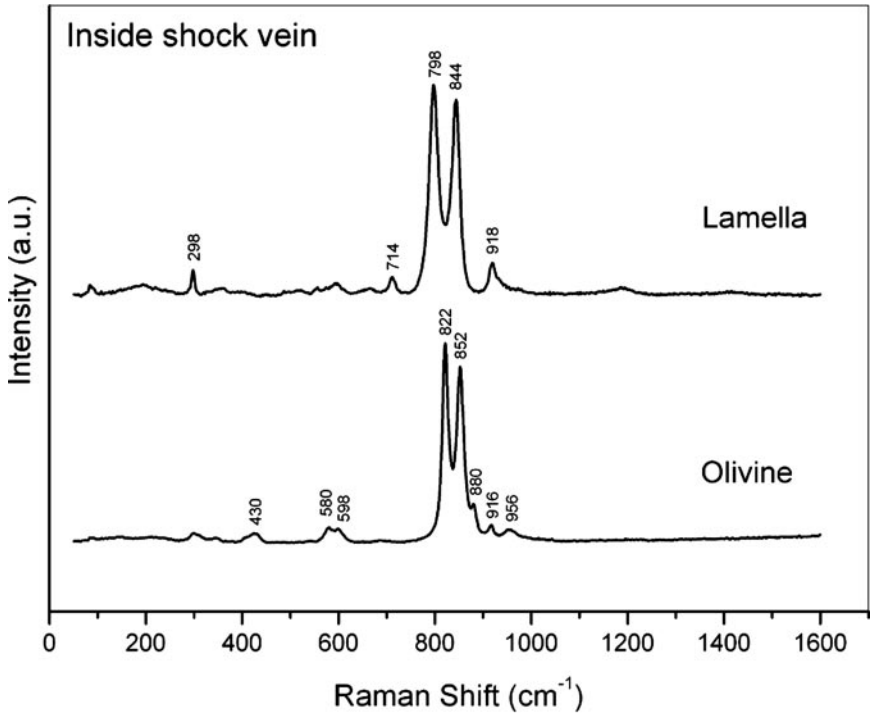

Fig. 3. Raman spectra from a porphyroclastic lamellae-bearing olivine inside the shock vein. Raman spectrum of lamellae contains two strong bands at 798 and 844 cm^{-1} and a weak band at 298 cm^{-1} corresponding to ringwoodite and two weak bands at 714 and 918 cm^{-1} corresponding to wadsleyite. The spectrum of olivine matrix neighboring the lamellae consists of the bands at 430, 580, 598, 822, 852, 880, 916, and 956 cm^{-1}. a.u., arbitrary unit.

they are subjected to high temperatures and hydrostatic pressure conditions. Under the latter conditions the ringwoodite lamellae would grow by a diffusion-controlled mechanism. It also should be noted that phase transformation mechanism for small olivine grains in the shock veins is different from that in large olivine grains. The olivine grains less than $\approx$100 μm in size within the

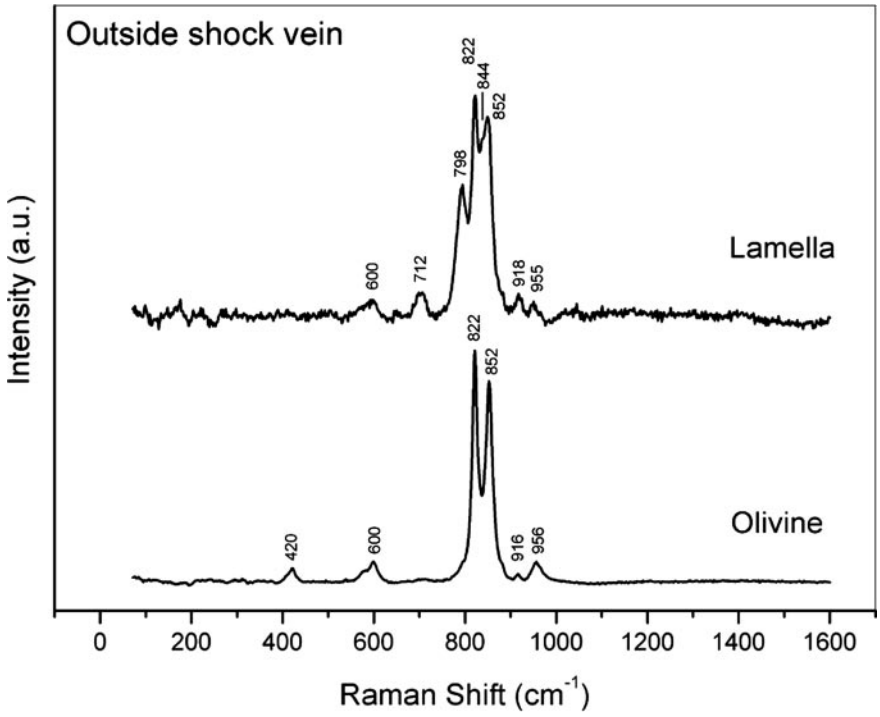

Fig. 4. Raman spectra from a lamellae-bearing olivine grain in the chondritic portion outside the shock vein. Raman spectrum obtained on the area from lamellae contains bands from several phases because the lamella is too thin. The strong bands at 798 and 844 cm^{-1} correspond to ringwoodite, the weak bands at 712 and 918 cm^{-1} correspond to wadsleyite, and bands at 600, 822, 852, and 955 cm^{-1} correspond to olivine matrix surrounding the lamellae. The spectrum of olivine matrix neighboring the lamellae contains the characteristic bands of olivine at 420, 600, 822, 852, 916, and 956 cm^{-1}. a.u., arbitrary unit.

shock veins of Sixiangkou meteorite were transformed mostly into polycrystalline aggregates of ringwoodite with triple junctions (4) with phase transitions commencing at grain boundaries because the grains were immediately heated to a very high temperature, and the pressure-temperature conditions largely overstepped the equilibrium phase boundary of ringwoodite and resulted in higher nucleation rate.

For the porphyroclastic grains of olivine in the shock veins, the thicker and higher densities of lamellae at the rim of olivine grains than in their interior indicate that temperature plays an important role in promoting an intracrystalline ringwoodite transformation in olivine. The surface layers of porphyroclastic grains of olivine enclosed by chondritic melt must have been heated to a higher temperature than their interiors, thus producing thicker and higher densities of lamellae at the rims of grains. Kerschhofer *et al.* (12) experimentally investigated the growth rates of ringwoodite lamellae along [100] of olivine at pressures 18–20 GPa and temperatures from 900°C to 1,100°C. Using the data of Kerschhofer *et al.* (12), we calculated the growth rates to be on the orders of 10^{-8} m/s at 1,500°C and 10^{-7} m/s at 1,700°C. Assuming that porphyroclastic grains of olivine inside the shock veins were heated to a temperature of 1,700°C at the rim and 1,500°C in the interior, the ringwoodite lamellae could grow to a thickness of 1.5 μm at the rim and 0.2 μm in the interior in a few seconds.

Our observations indicate that most troilite and iron-nickel metal-sulfide grains in the chondritic portion >100 μm away from the shock veins were not molten, thus indicating that the shock-induced temperature did not exceed 1,100°C. The existence of ringwoodite lamellae in olivine in these chondritic areas suggests that an intracrystalline ringwoodite transformation did take place in olivine at a lower temperature (<1,100°C). There is a pressure and temperature gradient from the shock vein toward neighboring chondritic portion. Provided the pressure and temperature in chondritic areas were ≈18 GPa and 1,100°C, a time duration up to several hours would be necessary to grow a ringwoodite lamella to a thickness of 0.5 μm, if we adopt an estimation of growth rates of lamellae by using the experimental data of Kerschhofer *et al.* (12).

The occurrence of ringwoodite lamellae in olivine shows that a longer duration than previously assumed of high pressure and temperature locally prevailed in the shocked meteorite, especially along the shock veins. Although a discrepancy may appear in estimated time duration of high pressure and temperature required to grow ringwoodite lamellae inside and outside the shock veins, our study suggests that the pressure-temperature condition available for an intracrystalline olivine–ringwoodite transformation in meteorite might last at least for several seconds. Conversely, although a number of experimental studies have supported that the intracrystalline transformation of olivine to ringwoodite in the subducting lithospheric slabs takes place along the (100) plane of olivine, our results suggest that the ringwoodite lamellae parallel to the {101} planes of olivine may develop in regions at higher shear stress and temperature than that parallel to the (100) plane of olivine. Therefore, it is worthwhile to conduct further experimental investigation for the pressure-temperature conditions to explore the mechanisms necessary for the production of intracrystalline high-pressure phase transformation along the {101} planes of olivine. In any case, our study demonstrates the existence of two distinct mechanisms of olivine–ringwoodite phase transformations in shocked chondrites: (*i*) lamellar intracrystalline intergrowth along (101) or (100) in large olivine grains in two distinct settings and pressure-temperature conditions, and (*ii*) polycrystalline aggregates of ringwoodite with triple junctions (4) with phase transitions commencing at grain boundaries in grains <100 μm in diameter.

It was considered that olivine might survive metastably in the wedge-shaped region within the cold subducting lithospheric slabs at depths from 400 to 700 km (27). The state of stress and temperature in different slabs are related to the convergence rates and the thermal gradients of slabs (8, 28). If a subducting slab is subjected to a higher temperature and stress, the {101} planar defects might be produced in large grains of olivine, and these defects subsequently would act as nucleation sites for ringwoodite lamellae. The (100) planar defects and ringwoodite lamellae also could be produced, assuming that these slabs are subjected to a lower stress and temperature (6, 10–12, 14, 18). However, our results also suggest that both intracrystalline olivine–ringwoodite phase transition mechanisms probably could occur in different regions in the same subducting slab where different degrees of stress and temperature prevail.

We thank two anonymous reviewers for constructive comments. M.C. was supported by the Chinese Academy of Sciences (Hundred Talents Program, Grants KZCX3-SW-123 and KJCX2-SW-NO3) and the National Natural Science Foundation of China.

1. Price, G. D., Putnis, A. & Agrell, S. O. (1979) *Contrib. Miner. Petrol.* **71,** 211–218.
2. Putnis, A. & Price, G. D. (1979) *Nature* **280,** 217–218.
3. Madon, M. & Poirier, J. P. (1983) *Phys. Earth Planet. Inter.* **33,** 31–44.
4. Chen, M., Sharp, T. G., El Goresy, A., Wopenka, B. & Xie, X. (1996) *Science* **271,** 1570–1573.
5. Sung, C. M. & Burns, R. G. (1976) *Earth Planet. Sci. Lett.* **32,** 165–170.
6. Burnley, P. C. & Green, H. W. (1989) *Nature* **338,** 753–756.
7. Green, H. W. & Burnley, P. C. (1989) *Nature* **341,** 733–737.
8. Rubie, D. C. & Ross, C. R. (1994) *Phys. Earth Planet. Inter.* **86,** 223–241.
9. Stein, S. A. & Rubie, D. C. (1999) *Science* **286,** 909–910.
10. Kerschhofer, L., Sharp, T. G. & Rubie, D. C. (1996) *Science* **274,** 79–81.
11. Kerschhofer, L., Dupas, C., Liu, M., Sharp, T. G., Durham, W. B. & Rubie, D. C. (1998) *Miner. Mag.* **62,** 617–638.
12. Kerschhofer, L., Rubie, D. C., Sharp, T. G., McConnell, J. D. C. & Dupas, C. (2000) *Phys. Earth Planet. Inter.* **121,** 59–76.
13. Burnley, P. C. (1995) *Am. Miner.* **80,** 1293–1301.
14. Martinez, I., Wang, Y., Guyot, F. & Liebermann, R. C. (1997) *J. Geophys. Res.* **102,** 5265–5280.
15. Lacam, A., Madon, M. & Poirier, J. P. (1980) *Nature* **288,** 155–157.
16. Boland, J. N. & Liu, L. G. (1983) *Nature* **303,** 233–235.
17. Madon, M., Guyot, F., Peyronneau, J. & Poirier, J. P. (1989) *Phys. Chem. Miner.* **16,** 320–330.
18. Wang, Y., Martinez, I., Guyot, F. & Liebermann, R. (1979) *Science* **275,** 510–513.
19. Poirier, J. P. (1981) *Phys. Earth Planet. Inter.* **26,** 179–187.
20. Guyot, F., Boyer, H., Madon, M., Velde, B. & Poirier, J. P. (1986) *Phys. Chem. Miner.* **13,** 91–95.
21. McMillan, P. F. & Akaogi, A. (1987) *Am. Miner.* **72,** 361–364.
22. Ashworth, J. R. & Barber, D. J. (1975) *Earth Planet. Sci. Lett.* **27,** 43–50.
23. Raleigh, C. B. (1968) *J. Geophys. Res.* **73,** 5391–5406.
24. Carter, N. L. (1971) *J. Geophys. Res.* **76,** 5514–5540.
25. Sung, C. M. & Burns, R. G. (1978) *Phys. Chem. Miner.* **2,** 177–197.
26. Stöffler, D., Keil, K. & Scott, E. R. D. (1991) *Geochim. Cosmochim. Acta* **55,** 3845–3867.
27. Frohlich, C. (1994) *Nature* **368,** 100–101.
28. Peacock, S. M. & Wang, K. (1999) *Science* **286,** 937–939.